Received: 25 February 2022 | Revised: 29 January 2023 | Accepted: 9 February 2023

DOI: 10.1111/ter.12645

RESEARCH ARTICLE

Terra Nova WILEY

Brittle basement deformation during the Caledonian Orogeny observed by K-Ar geochronology of illite-bearing fault gouge in west-central Sweden

Bjarne Almqvist[1] | Roelant van der Lelij[2] | Karin Högdahl[1] | Rodolphe Lescoutre[1] | Jasmin Schönenberger[2] | Haakon Fossen[3] | Håkan Sjöström[1] | Christopher Juhlin[1] | Stefan Luth[4] | Susanne Grigull[4,5] | Giulio Viola[6]

[1]Department of Earth Sciences, Uppsala University, Uppsala, Sweden

[2]Geological Survey of Norway, Trondheim, Norway

[3]Museum of Natural History, University of Bergen, Bergen, Norway

[4]Geological Survey of Sweden, Uppsala, Sweden

[5]Svensk Kärnbränslehantering AB (SKB), Solna, Sweden

[6]Department of Biological, Geological and Environmental Sciences, University of Bologna, Bologna, Italy

Correspondence
Bjarne Almqvist, Department of Earth Sciences, Uppsala University, Villavägen 16, 75236 Uppsala, Sweden.
Email: bjarne.almqvist@geo.uu.se

Funding information
Geological Survey of Sweden

Abstract

This study presents K-Ar ages of illite-bearing fault gouges in crystalline basement in central-western Sweden. Samples were taken from two faults that localized brittle deformation marginal to and within mafic dikes that intruded Paleoproterozoic granitoids. K-Ar ages from 10 separated grain fractions span from 823 to 392 Ma. Older ages obtained (823–477 Ma) were influenced by a mixture of illite and K-feldspar; the latter likely formed during a hydrothermal event prior to faulting. The remaining ages (442.1 ± 9.7 to 391.7 ± 6.1 Ma) were obtained from fractions from both faults hosting only authigenic illite and show that illite crystallized during the Scandian phase of the Caledonian orogeny. These results indicate that previously presumed autochthonous Caledonian basement was involved in continental contraction and subsequent collapse of the Caledonian orogen, influencing both the mode and depth of penetration of deformation into Baltica.

1 | INTRODUCTION

Cratonic nuclei forming the continental cores are considered to have been stable for billions of years. There is, however, limited information regarding their brittle structural evolution and deformation history (e.g. Tillberg et al., 2020, 2021). Faults in continental interiors provide a possibility to understand how brittle deformation has affected continent interiors. Such deformation can, for example result from far-field stresses generated at plate boundaries during orogeny (Goodfellow et al., 2017; Pinet, 2015; van der Pluijm et al., 1997). The overall orogenic deformation style generally depends on the position in the orogen (Fossen, 2016). Whereas the collision zone is commonly characterized by pervasive, medium- to high-grade ductile deformation, the foreland and plate interiors (autochthonous basement) are generally deformed by brittle structures at low-metamorphic grade. Assessing the relative involvement of the foreland and plate interior basement and their roles in orogeny is challenging. The localization, timing and distribution of deformation within orogenic foreland domains is complicated by the formation of multiple decoupling levels in the crust and/or structural inheritance, with the reactivation of pre-existing weak zones (e.g. Lacombe & Mouthereau, 2002; Mattila & Viola, 2014).

The Scandinavian Caledonides represent a well-exposed, deeply eroded Palaeozoic orogen comparable to the present-day Himalayas (Labrousse et al., 2010; Streule et al., 2010). Key questions concerning the orogen are how deformation was distributed in space and time during its evolution, and what role pre-existing structures played in shaping its architecture. In its external part, Cambrian shales acted as a major décollement level during the eastward transport of the overlying nappes (e.g. Gee, 1978; Rice & Anderson, 2016). However, seismic reflection imaging across the central Scandinavian Caledonides shows a pervasively reflective upper crust, down to at least 15 km present depth, characterized by sub-horizontal and west-dipping reflectors (Hurich et al., 1989; Juhlin et al., 2016; Juhojuntti et al., 2001; Palm et al., 1991). These reflectors are intriguing because they occur under the shale décollement and deep drilling indicated that they are likely to originate from mafic intrusions (Lorenz et al., 2022).

2 | GEOLOGICAL SETTING

The crystalline basement in central Scandinavia east of the Caledonian front is dominated by 1.88–1.74 Ga Svecokarelian granitoids (Figure 1a; Figure S1); in regard to the Caledonian orogeny, the granitoids are considered autochthonous. We studied two faults within these granitoids (Figure 1b,c; Figure S2), both <10 km from the front. Faulting localized mainly at the margins and within dolerite dikes (Figure 1b,c) of the ca. 1250–1270 Ma Central Scandinavian Dolerite Group (CSDG; Gorbatschev et al., 1979; Söderlund et al., 2006). Undeformed CSDG dikes east of the Caledonian front mainly comprise unaltered plagioclase, clinopyroxene and altered orthopyroxene (Figure S5a–d).

Samples KH1811 and KH1809C were collected from a shallowly W-NW dipping fault and from a steeply W-dipping fault, respectively, which nucleated marginal to and within mafic intrusions (Figure 1b,c). The shallow-dipping intrusion is ca. 0.4 m thick with top-to-the SE offset inferred by Riedel shears and thin shear bands in the host granitoid (Figure S4) as well as shear-sense indicators in thin sections (Figure S5e,f). For the steeply oriented fault, of ca. 0.5 m thickness, a dominantly west-down (normal) movement sense is inferred from the fault orientation and diffuse shear bands.

3 | METHODOLOGY

3.1 | Sample preparation

Bulk samples were submerged in deionized water and disaggregated using >100 freeze–thaw cycles. Size fractions of <0.1, 0.1–0.4, 0.4–2, 2–6 and 6–10 μm were then separated using gravity settling in cylinders for the >2 μm fractions, and continuous flow centrifugation for the <2 μm fractions. The fractions were collected with a high-speed fixed angle centrifuge and dried in an oven at 50°C.

3.2 | X-ray diffraction and K-Ar dating of clay mineral fraction

The mineralogy of all size fractions was studied with X-ray diffraction (XRD). Randomly oriented samples were prepared by side-loading and analysed with a Bruker D8 Advance X-ray diffractometer with a Cu X-ray tube (40 kV/40 mA) and Lynxeye XE detector. Mineral quantification was performed using Rietveld modelling with the TOPAS 5 software. Illite crystallinity (Kübler Index) was determined from the full width at half maximum (FWHM) of the 10 Å peak and standardized according to Warr (2018) and Warr and Rice (1994).

The homogenized clay materials and standards were packed in weighted molybdenum envelopes. Argon isotopes were determined on an IsotopX NGX multicollector noble gas mass spectrometer using faraday cups fitted with $10^{12}\,\Omega$ amplifiers, except for ^{40}Ar, which was measured using a faraday cup fitted with a $10^{11}\,\Omega$ amplifier. Potassium concentrations were determined by digesting aliquots of ~50 mg of sample material in $Li_2B_4O_7$ flux at a temperature of 1000 ± 50°C in palladium crucibles. The resulting glass was subsequently dissolved in HNO_3 and analysed on a Perkin Elmer Optima 4300 DV ICP-OES. 1σ uncertainties depend on the sample weight and its K concentration and are better than 1.5% relative for pure illite/mica, as determined by repeated measurements of several geological standards. K-Ar ages were calculated using the ^{40}K decay constants, abundance and branching ratio of Steiger and Jäger (1977). Atmospheric argon corrections were performed using the relative abundances of ^{40}Ar, ^{38}Ar and ^{36}Ar of Lee et al. (2006; $^{40}Ar/^{36}Ar = 298.56 \pm 0.31$). Further details on the XRD and K-Ar analyses are given in the supplementary material.

4 | RESULTS

4.1 | XRD and sample mineral composition

The samples have similar mineralogy and clay mineral concentrations (Figure 2a,b; Table S1, Figure S3). The separated fine fractions consist mainly of chlorite + smectite and illite/muscovite, with lesser amounts of quartz, K-feldspar and plagioclase, and minor amphibole and hematite. Quartz and feldspar are more abundant in coarse-grained fractions, but nearly absent in the <0.1 and 0.1–0.4 μm fractions. The illite/muscovite concentration is higher in KH1811. The 1 M polytype is the sole type of illite identified in the fine grain fractions, ranging from <0.1 μm up to 2 μm. In sample KH1809C, there are indications that the $2M_1$ illite polytype is present in the 2–6 and 6–10 μm grain-size fractions; the 10 Å peaks are well defined and the typical 2 M1 peak at 2.8 Å is clearly visible. Note that it was not possible to evaluate the modal mineral composition in the <0.1 μm fraction of KH1809C because of an insufficient amount of sample material, but the separated fraction could still be used for K-Ar dating.

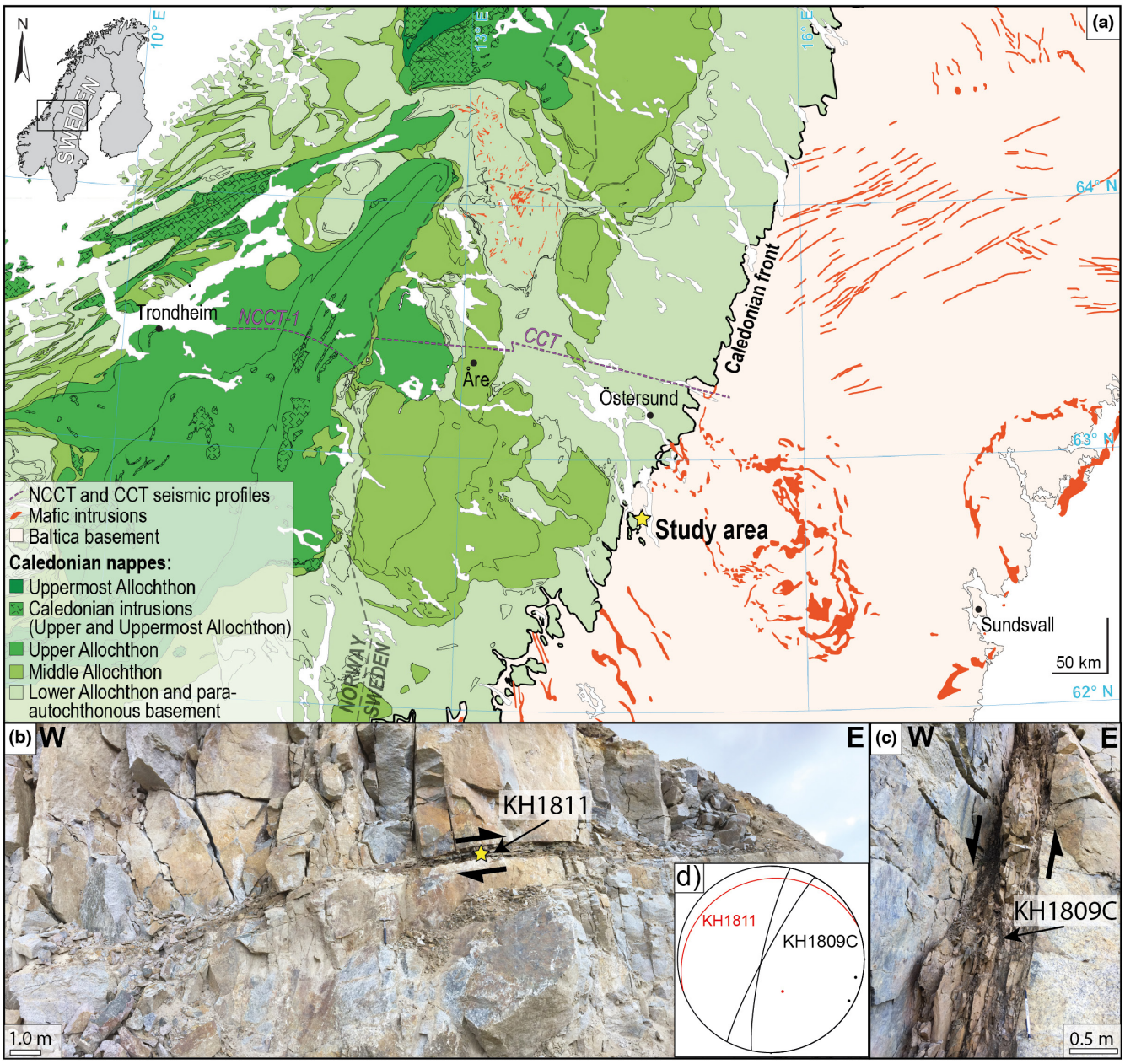

FIGURE 1 (a) Map of the Baltica basement and the main tectonic units of the central Scandinavian Caledonides (modified from Robinson et al., 2014); CSDG mafic intrusions are shown in red (based on databases from the Geological Survey of Sweden). The CCT and NCCT-1 seismic profiles across the central Scandinavian Caledonides are indicated by the dashed purple line (Hurich et al., 1989; Palm et al., 1991); (b, c) field pictures of the faulted intrusions hosted by granitoids. (b) Low-angle west-dipping thrust fault showing brittle deformation localized along a ca. 0.4 m thick dolerite dike with sample location of KH1811; (c) steeply oriented, west-dipping fault with inferred west side down movement with sample location of KH1809C. (d) Equal-area projection showing the fault planes (dip and dip directions) and poles to fault planes.

4.2 | K-Ar geochronology

The K-Ar results are summarized in Table 1 and shown in Figure 2c. Sample KH1809C shows ages ranging from 822.7±11.6 Ma to 442.1±9.7 Ma, whereas KH1811 shows a narrower distribution of ages, ranging from 652.2±8.9 Ma to 391.7±6.1 Ma (Figure 2c; Table 1). The coarser grain-size fractions invariably yield older ages, whereas the finest fractions yield the youngest ages. Sample KH1809C yielded older ages than KH1811, for all grain size fractions. Note that the K-feldspar to illite ratio is higher for all grain-size fractions of KH1809C.

5 | DISCUSSION AND CONCLUSIONS

5.1 | Origin of the clay mineral fraction in the faulted dikes

Whether illite formed authigenically during faulting or whether it is at least in part protolithic or related to other geological events that are not necessarily tied to deformation is an important constraint on interpreting the results. The $2M_1$ polytype is considered detrital in fault rocks, because it typically forms at temperatures

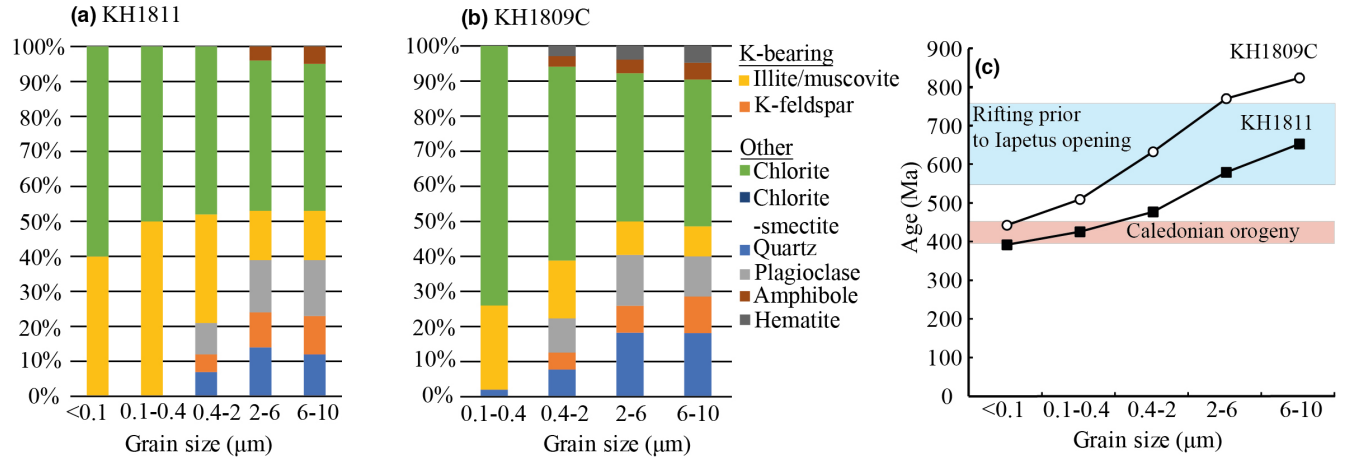

FIGURE 2 (a, b) Mineral modal composition from XRD for samples KH1811 and KH1809C. Note that the finest fraction (<0.1 μm) did not yield a discernable modal composition from XRD in sample KH1809C; (c) K-Ar geochronology results as a function of the separated clay mineral grain-size fraction (1σ standard deviations are smaller than the symbol representing the data point).

TABLE 1 Summary of K-Ar geochronology results

Sample parameters		^{40}Ar				K			Age data
Sample name	Fraction (μm)	Mass (mg)	mol/g	σ (%)	^{40}Ar* %	Mass (mg)	Wt%	σ (%)	Age (Ma)
KH1811	<0.1	1.578	2.423 E-09	0.34	90.8	14.6	3.193	1.69	391.7
	0.1–0.4	1.470	3.020 E-09	0.35	93.5	49.9	3.631	1.41	425.3
	0.4–2	1.702	2.792 E-09	0.33	94.0	49.9	2.951	1.51	476.7
	2–6	1.848	2.815 E-09	0.31	94.4	50.9	2.377	1.59	579.0
	6–10	1.636	3.281 E-09	0.33	94.0	50.1	2.408	1.60	652.2
KH1809C	<0.1	1.022	1.046 E-09	0.48	90.3	17.4	1.204	2.44	442.1
	0.1–0.4	1.266	1.708 E-09	0.40	93.5	50.0	1.676	1.76	508.6
	0.4–2	1.860	2.178 E-09	0.31	95.8	50.1	1.660	1.76	632.0
	2–6	3.374	2.869 E-09	0.25	97.3	50.0	1.725	1.75	769.3
	6–10	1.896	3.218 E-09	0.31	97.8	50.0	1.780	1.73	822.7

that exceed 280°C (van der Pluijm et al., 2006). By contrast, the 1 M polytype forms at low-*T* diagenetic conditions and is considered to have formed authigenically in response to faulting (Hueck et al., 2022; van der Pluijm et al., 2006). Sample KH1811 lacks the typical $2M_1$ polytype peak at 2.8 Å, indicating that this sample exclusively contains the 1 M polytype. By contrast, the presence of $2M_1$ polytype illite/muscovite in the two coarsest size fractions of sample KH1809C, shown by the well-defined 10 Å peak and the presence of the 2.8 Å peak, implies that these fractions contain illite/muscovite of a potentially inherited origin (Grathoff & Moore, 1996). Alternatively, the $2M_1$ polytype may have originated from hydrothermal fluids or faulting at higher temperatures (Figure S2g,h; Table 2). Notably, the coarser grain size fractions contain up to 10 vol.% K-feldspar, which is likely to have influenced the ages of the coarser fractions where K-feldspar concentrations are comparable to that of illite. The finest grain size fractions, 0.1–0.4 μm fraction for sample KH1809C and the <0.1 μm and 0.1–0.4 μm fractions for sample KH1811, are interpreted to have formed authigenically during faulting because of the predominance of the 1 M illite polytype and absence of K-feldspar. As such their growth ages are taken to represent the timing of slip events along the sampled faults, according to the age attractor model of Torgersen et al. (2014, 2015) and Viola et al. (2016). It cannot be excluded that a very small fraction of K-feldspar (<1%) could be present in the fine-grained samples, but in concentrations below the detection limit of XRD. Age models with mixed contributions of illite and K-feldspar are provided in Material S3. These models indicate that the maximum ages of K-feldspar range from 1000 to 1250 Ma, and hence do not originate from the host granitoids (~1850–1800 Ma), since modelled values for K-feldspar become too old in comparison with observed ages (see Figure S7). The presence of up to 1% of hydrothermal origin K-feldspar in the most fine-grained portions of samples, with a maximum age of ~1250 Ma, would skew the resultant ages less than 10 Ma. This suggests that a non-detectible fraction of K-feldspar, in the XRD measurements, would contribute little to the observed ages and

TABLE 2 Summary of potential tectonic/hydrothermal events that produced growth of illite and K-feldspar.

Age (Ma)[a]	Tectonic event[a]	Product/consequence of the event
2000–1800	Svecokarelian orogeny	Too old for K-feldspar or illite (Material S3)
1700–1400	Continental magmatism and intracratonic rifting (Trans-Scandinavian igneous belt and Mesoproterozoic events)	Too old for K-feldspar or illite (Material S3)
~1270–1250 1140 980–950	Intracratonic rifting events	Possible timing of K-feldspar (Material S3)
900–1000	Sveconorwegian orogeny	Possible timing of K-feldspar
1000–600	Tonian—Cryogenian rifting	Possible timing of coarse-grained illite, and youngest ages of K-feldspar (Material S3)
430–400	Caledonian orogeny	Illite formation (finer grain size fractions)
<400	Caledonian exhumation, or end-stage of Caledonian Scandian collision phase; Variscan orogeny	Illite formation in finest grain size fraction of sample KH1811

[a]Tectonic events and range in ages are used from Stephens and Bergman Weihed (2020).

the presence of K-feldspar is not responsible for differences in ages observed for the most fine-grained fractions in either sample.

5.2 | Brittle deformation in the Baltica basement during Caledonian orogeny

The older ages observed in both samples show a portion of K-feldspar mixed with illite, likely originating from hydrothermal fluids. By contrast, the younger ages from 442 to 392 Ma, result solely from the 1 M illite polytype and give Caledonian signatures, where faulting occurred prior to and during continent–continent collision. Table 2 provides an overview of the potential tectonic and hydrothermal events that were likely to have created illite and K-feldspar. The limitation of the current dataset is recognized, in terms of the limited number of samples (two samples with 10 size fractions) and the possibility for mixed ages in the separated grain-size fractions. A mixture of ages is suggested by the absence of a plateau in the ages presented in Figure 2 (i.e. inclined age spectra). However, the K-Ar ages show small standard deviations, which indicate limited mixing of K-Ar ages within the same grain-size fraction. Furthermore, samples from both faults demonstrate that Caledonian age fault movement took place in the basement rocks.

The youngest ages recorded are from the gouge of the shallow NW-dipping fault (KH1811), where a top-SE thrust sense of movement is recorded. The older age of ~442 Ma pre-dates the final stage of continent–continent collision of Baltica and Laurentia (e.g. Torsvik et al., 1996, 2012), and is found on the steep, apparent normal, W-dipping fault (KH1809C). This age would correspond to localized high-grade and high-pressure metamorphism of subducted continental crust in the central Scandinavian Caledonides and slightly pre-dates widespread magmatic activity (440–430 Ma) along the entire orogen (Slagstad & Kirkland, 2018). How then did the deformation front reach the sample localities far into Sweden in the early Silurian, (~442 Ma)? One explanation is that stresses were transmitted far eastwards because of the cold and rigid basement during closure of the Iapetus Ocean and initial continental collision (e.g. Fossen et al., 2017), which would be physically manifested through faulting of the Baltica basement. The youngest age observed, 391.7 ± 6.1 Ma for sample KH1811, is challenging to relate to thrusting (e.g., Fossen & Dunlap, 1998), as this age is younger than the Scandian collision phase of the Caledonian orogeny. This age coincides with Caledonian orogenic collapse, possibly related to the Variscan orogeny from the south (Table S2; Rey et al., 1997). However, there are geochronology results that indicate that the Scandian phase of the Caledonian collision may have of lasted until 385–380 Ma, based on Rb-Sr dating of mylonites in the Kalak nappe (Roberts & Sundvoll, 1990) and U–Pb dating of zircons from gneiss mylonites from central Jämtland that grew in response to metamorphic heating (Högdahl et al., 2001).

Strain localization marginal to and within dikes may have been important during deformation of the Baltica basement. The generally west-dipping structures observed in the eastern parts of the CCT and CSP seismic profiles (Juhlin et al., 2016; Juhojuntti et al., 2001) are in a favourable orientation to have accommodated strain and been (re)activated. The reflection seismic images indicate that the CSDG and potentially older dikes (Lescoutre, Söderlund, et al., 2022) are distributed in the basement, at least at and east of the Caledonian front and have been inferred to occur, based on geochemistry, as far west as the Tømerrås basement window in Norway (Johansson, 1980). Greiling et al. (2007) noted a progressive increase in faulting and deformation, involving the CSDG intrusions, from the exterior to the interior of the orogen. Importantly, they noted a striking rheological contrast between dikes and the granitic basement, where the former is considerably less competent at low grade metamorphic conditions. In our study area, the dikes never experienced deformation at high metamorphic grade conditions, and the rheological contrast between dike and host rock is the likely reason for strain localization at the

margin of the dikes (e.g. Wilson et al., 2020). Recently, Lescoutre, Almqvist, et al. (2022) indicate that contractional deformation occurred in the basement underneath the allochthonous cover, where mafic sheets likely guided the localization. The partial kinematic restoration of Lescoutre, Almqvist, et al. (2022), based on seismic reflection profiles, provide a minimum displacement of ~6 km along one restoration plane in the crystalline basement, suggesting that shortening in the basement is significant.

The observations and geochronology results presented here yield three conclusions. First, although it has been previously shown the crystalline basement was involved in (mostly ductile) Caledonian deformation in the hinterland (e.g. Bjørlykke & Olesen, 2019), we here show that basement at the foreland is deformed during the orogeny. The results presented in this study provides the first direct evidence in central Scandinavia for brittle deformation, where the mode of faulting and the age of the fault events can be associated. This is in contrast to the studies of Tillberg et al. (2020, 2021), where the mode of faulting could be indirectly associated with mineralization events that took place during the Caledonian orogeny. Second, any estimate of continental contraction must therefore include deformation in the foreland and crystalline basement, and not only in allochthonous units and along the décollement. Such a case has recently been illustrated by Duvall et al. (2020), who showed that blind faults occurring in the Indian basement, south of the Himalayan Main Frontal Thrust, likely lead to an underestimation of the collisional convergence and rate of convergence. Third, the accommodation of deformation in the basement away from the main collision zone indicates that stress is transmitted into the craton from the collision zone. Van der Pluijm et al. (1997) have indicated that mountain belts are in fact 'filters' of stress and that the specific style and properties of convergence are not reflected in the stress state of continental interiors. Differential stresses generated by orogenic collision zones, on the order to ~20 MPa, could be transmitted several thousand kilometres into the continents. These stresses could then be responsible for (re-)activation and failure of favourably oriented structures, for example along pre-existing faults, but also marginal to and in sills and dikes, such as exists near and underneath the Caledonian foreland in the crystalline basement of Baltica. Indeed, Caledonian age fault gouge have been observed far from the orogenic front, as reported by Almqvist et al. (2019) and Tillberg et al. (2020, 2021), suggesting that significant far-field stresses into the Baltic Craton resulted from the Caledonian Orogeny.

ACKNOWLEDGEMENTS

This study was made possible through financial support of the Swedish Geological Survey, grant 36-1940/2017. X. Ruikai Xie at NGU laboratory is thanked for careful K analysis. We are greatly indebted to the review of Hugh Rice, as well as an anonymous reviewer, which improved the manuscript. We also acknowledge the support of the associate editor Igor Villa and editor Klaus Mezger.

DATA AVAILABILITY STATEMENT

The data that supports the findings of this study are available in the supplementary material of this article

REFERENCES

Almqvist, B, van der Lelij, R., Grigull, S., Högdahl, K., Luth, S., Schönenberger, J., Viola, G. (2019). Dating brittle deformation of the Söderström fault, Stockholm, Central Sweden. *Geophysical Research Abstracts*, 21, EGU2019-11026-2.

Bjørlykke, A., & Olesen, O. (2019). Caledonian deformation of the Precambrian basement in southeastern Norway. *Norwegian Journal of Geology*, *98*, 1–16. https://doi.org/10.17850/njg98-4-05

Duvall, M. J., Waldron, J. W. F., Godin, L., & Najman, Y. (2020). Active strike-slip faults and an outer frontal thrust in the Himalayan foreland basin. *Proceedings in the National Academy of Sciences of the United States of America*, *117*, 17615–17621.

Fossen, H. (2016). *Structural geology* (2nd ed., p. 524). Cambridge University Press.

Fossen, H., Cavalcante, G. C., & Paes de Ameida, R. (2017). Hot versus cold orogenic behavior: Comparing the Araçuaí-West Congo and the Caledonian orogens. *Tectonics*, *36*, 2159–2178.

Fossen, H., & Dunlap, W. J. (1998). Timing and kinematics of Caledonian thrusting and extensional collapse, southern Norway: Evidence from $^{40}Ar/^{39}Ar$ thermochronology. *Journal of Structural Geology*, *20*, 765–781.

Gee, D. (1978). Nappe displacement in the Scandinavian Caledonides. *Tectonophysics*, *47*, 393–394.

Goodfellow, B. W., Viola, G., Bingen, B., Nuriel, P., & Kylander-Clark, A. R. C. (2017). Paleocene faulting in SE Sweden from U-Pb dating of slickenfibre calcite. *Terra Nova*, *29*, 321–328. https://doi.org/10.1111/ter.12280

Gorbatschev, R., Solyom, Z., & Johansson, I. (1979). The central Scandinavian dolerite Group in Jämtland, Central Sweden. *Geologiska Föreningen i Stockholm Förhandlingar*, *101*, 177–190.

Grathoff, G., & Moore, D. M. (1996). Illite polytype quantification using WILDFIRE© calculated X-ray diffraction patterns. *Clays and Clay Minerals*, *44*, 835–842.

Greiling, R. O., Grimmer, J. C., De Wall, H., & Björk, L. (2007). Mesoproterozoic dyke swarms in foreland and nappes of the central Scandinavian Caledonides: Structure, magnetic fabric, and geochemistry. *Geological Magazine*, *144*, 525–546.

Högdahl, K., Gromet, L. P., & Broman, C. (2001). Low P-T Caledonian resetting of U-rich Paleoproterozoic zircons Central Sweden. *American Mineralogist*, *86*, 534–546.

Hueck, M., Wemmer, K., Ksienzyk, A. K., Kuehn, R., & Vogel, N. (2022). Potential, premises, and pitfalls of interpreting illite argon dates – A case study from the German Variscides. *Earth-Science Reviews*, *232*, 104133.

Hurich, C. A., Palm, H., Dyrelius, D., & Kristoffersen, Y. (1989). Deformation of the Baltic continental crust during Caledonide intracontinental subduction: Views from seismic reflection data. *Geology*, *17*, 423–425.

Johansson, L. (1980). Petrochemistry and regional tectonic significance of metabasites in basement windows of the central Scandinavian Caledonides. *Geologiska Föreningen i Stockholm Förhandlingar*, *102*, 499–514.

Juhlin, C., Hedin, P., Gee, D. G., Lorenz, H., Kalscheuer, T., & Yan, P. (2016). *Seismic imaging on the eastern Scandinavian Caledonides: Siting the 2.5 km deep COSC-2 borehole, central Sweden* (Vol. *7*, pp. 769–787). Solid Earth.

Juhojuntti, N., Juhlin, C., & Dyrelius, D. (2001). Crustal reflectivity underneath the Central Scandinavian Caledonides. *Tectonophysics*, *334*, 191–210.

Labrousse, L., Hetényi, G., Raimbourg, H., Jolivet, L., & Andersen, T. B. (2010). Initiation of crustal-scale thrusts triggered by metamorphic reactions at depth: Insights from a comparison between the Himalayas and Scandinavian Caledonides. *Tectonics*, *29*(5). https://doi.org/10.1029/2009TC002602

Lacombe, O., & Mouthereau, F. (2002). Basement-involved shortening and deep detachment tectonics in forelands of orogens: Insights

from recent collision belts Taiwan, Western Alps, Pyrenees. *Tectonics*, *21*, 12-1–12-22. https://doi.org/10.1029/2001TC9010118

Lee, J.-Y., Marti, K., Severinghaus, J. P., Kawamura, K., Yoo, H.-S., Lee, J. B., & Kim, J. S. (2006). A redetermination of the isotopic abundances of atmospheric Ar. *Geochimica et Cosmochimica Acta*, *70*, 4507–4512.

Lescoutre, R., Almqvist, B., Koyi, H., Berthet, T., Hedin, P., Galland, O., Brahimi, S., Lorenz, H., & Juhlin, C. (2022). Large-scale flat-lying mafic intrusions in the Baltican crust and their influence on basement deformation during the Caledonian orogeny. *GSA Bulletin*, *134*, 3022–3048. https://doi.org/10.1130/B36202.1

Lescoutre, R., Söderlund, U., Andersson, J., Almqvist, B. (2022) 1.47 Ga and 1.27–1.26 Ga dolerite sheets within the basement underneath the east-central Scandinavian Caledonides. Geological Society of Sweden 150-year anniversary meeting, extended abstract.

Lorenz, H., Rosberg, J.-E., Juhlin, C., Klonowska, I., Lescoutre, R., Westmeijer, G., Almqvist, B. S. G., Anderson, M., Bertilsson, S., Dopson, M., Kallmeyer, J., Kück, J., Lehnert, O., Menegon, L., Pascal, C., Rejkjær, S., & Roberts, N. N. W. (2022). COSC-2—Drilling the basal décollement and underlying margin of paleocontinent Baltica in the Paleozoic Caledonide Orogen of Scandinavia. *Scientific Drilling*, *30*, 43–57.

Mattila, J., & Viola, J. (2014). New constraints on 1.7 Gyr of brittle tectonic evolution in southwestern Finland derived from a structural study at the site of a potential nuclear waste repository (Olkiluoto Island). *Journal of Structural Geology*, *67*, 50–74.

Palm, H., Gee, D., Dyrelius, D., and Björklund, L. (1991). A reflection seismic image of Caledonian structure in Central Sweden. Geological Survey of Sweden report. Ca 75.

Pinet, N. (2015). Far-field effects of Appalachian orogenesis: A view from the craton. *Geology*, *44*, 83–86.

Rey, P., Burg, J.-P., & Casey, M. (1997). The Scandinavian Caledonides and their relationship to the Variscan belt. *Geological Society of London Special Publication*, *121*, 179–200.

Rice, A. H. N., & Anderson, M. W. (2016). Restoration of the external Scandinavian Caledonides. *Geological Magazine*, *153*, 1136–1165.

Roberts, D., & Sundvoll, B. (1990). Rb-Sr whole-rock and thin-slab dating of mylonites from the Kalak thrust zone, near Børselv, Finnmark. *Norsk Geologisk Tidsskrift*, *70*, 259–266.

Robinson, P., Roberts, D., Gee, D. G., & Solli, A. (2014). A major synmetamorphic early Devonian thrust and extensional fault system in the mid Norway Caledonides: Relevance to exhumation of HP and UHP rocks. *Geological Society London, Special Publications*, *390*(1), 241–270.

Slagstad, T., & Kirkland, C. L. (2018). Timing of collision initiation and location of the Scandian orogenic suture in the Scandinavian Caledonides. *Terra Nova*, *30*, 179–188.

Söderlund, U., Elming, S.-Å., Ernst, R. E., & Schissel, D. (2006). The central Scandinavian dolerite group—Protracted hotspot activity or back-arc magmatism? Constraints from U-Pb Baddeleyite Geochronology and Hf Isotopic Data. *Precambrian Research*, *150*, 136–152.

Steiger, R. H., & Jäger, E. (1977). Subcommission on geochronology: Convention on the use of decay constants in geochronology and cosmochronology. *Earth and Planetary Science Letters*, *36*, 359–362.

Stephens, M. B., & Bergman Weihed, J. (2020). *Sweden: Lithotectonic framework, tectonic evolution and mineral resources* (p. 50). Geological Society, London, Memoirs.

Streule, M. J., Strachan, R. A., Searle, M. P., & Law, R. D. (2010). Comparing Tibet-Himalayan and Caledonian crustal architecture, evolution and mountain building processes. *Geological Society London, Special Publications*, *335*, 207–232.

Tillberg, M., Drake, H., Zack, T., Hogmalm, J., Kooijman, E., & Åström, M. (2021). Reconstructing craton-scale tectonic events via in situ Rb-Sr geochronology of poly-phased vein mineralization. *Terra Nova*, *33*, 502–510. https://doi.org/10.1111/ter.12542

Tillberg, M., Drake, H., Zack, T., Kooijman, E., Whitehouse, M. J., & Åström, M. E. (2020). In situ Rb-Sr dating of slickenfibres in deep crystalline basement faults. *Nature Scientific Reports*, *10*, 562. https://doi.org/10.1038/s41598-019-57262-5

Torgersen, E., Viola, G., Zwingmann, H., & Harris, C. (2014). Structural and temporal evolution of a reactivated brittle-ductile fault—Part II: Timing of fault initiation and reactivation by K-Ar dating of synkinematic illite/muscovite. *Earth and Planetary Science Letters*, *407*, 221–233.

Torgersen, E., Viola, G., Zwingmann, H., & Henderson, I. H. (2015). Inclined K-Ar age spectra in brittle fault gouges: Effects of fault reactivation and wall-rock contamination. *Terra Nova*, *27*, 106–113. https://doi.org/10.1111/ter.12136

Torsvik, T. H., Smethurst, M. A., Meert, J. G., Van der Voo, R., McKerrow, W. S., Brasier, M. D., Sturt, B. A., & Walderhaug, H. J. (1996). Continental break-up and collision in the Neoproterozoic and Palaeozoic—A tale of Baltica and Laurentia. *Earth-Science Reviews*, *40*, 229–258.

Torsvik, T. H., Van der Voo, R., Preeden, U., Mac Niocaill, C., Steinberger, B., Doubrovine, P. V., van Hinsbergen, D. J. J., Domeier, M., Gaina, C., Tohver, E., Meert, J. G., McCausland, P. J. A., & Cocks, R. (2012). Phanerozoic polar wander, paleogeography and dynamics. *Earth-Science Reviews*, *114*, 325–368.

van der Pluijm, B., Craddock, J. P., Graham, B. R., & Harris, J. H. (1997). Paleostress in Cratonic North America: Implications for deformation of continental interiors. *Science*, *277*, 794–796.

van der Pluijm, B., Vrolijik, P. J., Pevear, D. R., Hall, C. M., & Solum, J. (2006). Fault dating in the Canadian Rocky Mountains: Evidence for late cretaceous and early Eocene orogenic pulses. *Geology*, *34*, 837–840.

Viola, G., Scheiber, T., Fredin, O., Zwingmann, H., Margreth, A., & Knies, J. (2016). Deconvoluting complex structural histories archived in brittle fault zones. *Nature Communications*, *7*, 13448. https://doi.org/10.1038/ncomms13448

Warr, L. N. (2018). A new collection of clay mineral "crystallinity" index standards and revised guidelines for the calibration of Kübler and Árkai indices. *Clay Minerals*, *53*, 1–12.

Warr, L. N., & Rice, A. H. N. (1994). Interlaboratory standardization and calibration of clay mineral crystallinity and crystallite size data. *Journal of Metamorphic Geology*, *12*, 141–152.

Wilson, C. J. L., Vassallo, J. J., & Hoek, J. D. (2020). Rheological behaviour of mafic dykes deformed in a granite host, Wanna, Eyre Peninsula, South Australia. *Journal of Structural Geology*, *140*, 104164.

SUPPORTING INFORMATION

Additional supporting information can be found online in the Supporting Information section at the end of this article.

Data S1.

How to cite this article: Almqvist, B., van der Lelij, R., Högdahl, K., Lescoutre, R., Schönenberger, J., Fossen, H., Sjöström, H., Juhlin, C., Luth, S., Grigull, S., & Viola, G. (2023). Brittle basement deformation during the Caledonian Orogeny observed by K-Ar geochronology of illite-bearing fault gouge in west-central Sweden. *Terra Nova*, *00*, 1–7. https://doi.org/10.1111/ter.12645